7th Australian Conference on Laser Diagnostics in Fluid Mechanics and Combustion
Melbourne, Australia
9-11 December 2015

Towards capturing large scale coherent structures in boundary layers using particle image velocimetry.

C. M. de Silva[1], D. T. Squire[1], N. Hutchins[1] and I. Marusic[1]

Corresponding author: desilvac@unimelb.edu.au
[1]Department of Mechanical Engineering,
The University of Melbourne, Victoria 3010, Australia

Abstract

Here we describe the implementation of a large-scale multi-camera particle image velocity (PIV) measurement to resolve the large range of spatial scales prevalent in moderate to high Reynolds number turbulent boundary layers. The objective of these experiments is to capture instantaneous snapshots of recently discovered large coherent structures which are known to inhabit the log and outer regions of boundary layers, while still maintaining sufficient fidelity to resolve a large proportion of the smaller spatial scales that coexist. Measurements are conducted across friction Reynolds number range from $Re_\tau = 2000$ to 8000 in a planar PIV configuration on a streamwise/wall-normal plane with a streamwise field of view in excess of 14 boundary layer thicknesses. These datasets are supplemented by planar PIV measurements on a streamwise/spanwise plane which spans a similar streamwise extent. Flow statistics are compared to recent numerical simulation databases at moderate Re, and to well resolved single point hot-wire anemometry measurements at higher Re to validate and assess the quality of the PIV velocity fields. The results reveal good agreement and also indicate that a simple box filter approach can be used to estimate spatial attenuation for PIV measurements. Comparisons between the pre-multiplied energy spectra of the streamwise velocity fluctuations from the PIV and hotwire databases also show good agreement over the field of view when Taylor's frozen turbulence hypothesis is assumed.

Introduction

Over the last two decades, particle image velocimetry (PIV) has become increasingly popular for carrying out accurate multi-component, multi-dimensional spatial measurements of turbulent flows [2]. Although one can obtain higher signal-to-noise ratios and longer time-averaged signals from single point measurement techniques (e.g. hot-wire anemometry [5]), PIV provides spatial derivatives, flow visualisations and spatial correlations. To date, PIV is one of the few techniques that provides such spatial information in rapidly evolving flows and at a level of detail that was once considered achievable only in numerical simulations. PIV techniques can be categorised into measuring two- or three-component velocity vector fields in a plane and, more recently, over volumetric domains [16, 2]. One notable distinction between PIV techniques is the higher fidelity and larger spatial domains typically associated with planar techniques, albeit with substantially less information compared to volumetric techniques. The present study focuses on the implementation of a large-scale planar snapshot PIV configuration.

Among the many applications of PIV, turbulent flows still stand as one of the most demanding applications due to their wide range of length and time scales (see the recent review by [22]). A characteristic measure of the length-scale range in these flows is the Reynolds number (Re_τ), corresponding to the ratio between the largest and smallest length scales ($Re_\tau = \delta U_\tau/\nu$). However, to date, PIV measurements in turbulence, particularly at high Re_τ, are typically limited by the available dynamic spatial range (DSR), which denotes the ratio between the maximum and minimum resolvable length-scales. Here we utilise a multi-camera PIV setup that overcomes these issues and takes us one step closer in achieving good spatial resolution while maintaining a relatively large field of view.

Of particular interest in the present study is to capture instantaneous snapshots of recently discovered large structures which are known to inhabit the log and outer regions of boundary layers at moderate to high Re_τ [11]. These structures are known to exist in both internal and external wall-turbulence, and carry substantial proportions of Reynolds shear stress and turbulence production. They are also known to modulate the near-wall cycle [13] and influence interfacial bulging. Prior evidence of these structures has largely been provided by inferring spatial information from temporally resolved single-component point measurements using Taylor's frozen turbulence hypothesis [20]. However, this technique is limited, particularly over large spatial extents [10, 4]. Furthermore these large-scale motions are known to meander, which inhibits the accurate description of these structures via single point measurements. Large-scale PIV experiments, such as those presented herein, offer a promising approach to examine these large-scale motions. However, the approach is not without its own difficulties; these structures are known to commonly persist for streamwise distances exceeding ten boundary layer thicknesses ([11] reports streamwise coherent structures with lengths $> 20\delta$), requiring the use of multiple imaging sensors to obtain sufficient spatial resolution over such a large streamwise extent if one was to capture these structures using PIV.

Throughout this paper, the coordinate system x, y and z refers to the streamwise, spanwise and wall-normal directions, respectively. Corresponding instantaneous streamwise, spanwise and wall-normal velocities are represented by $\widetilde{U}$, $\widetilde{V}$ and $\widetilde{W}$, respectively, with the corresponding velocity fluctuations given by lower case letters. Overbars indicate averaged quantities, and the superscript + refers to normalisation by inner scales. For example, we use $l^+ = lU_\tau/\nu$ for length and $\widetilde{U}^+ = \widetilde{U}/U_\tau$ for velocity, where U_τ is the friction velocity and ν is the kinematic viscosity of the fluid.

Description of experiments

Facility and Instrumentation

The experiments described in this paper are performed in the High Reynolds Number Boundary Layer Wind Tunnel (HRNBLWT) at the University of Melbourne. The tunnel consists of a large development length of approximately 27m, offering the capability of achieving high Re_τ at relatively low freestream velocities. This provides a uniquely thick smooth-wall boundary layer at Re_τ up to 25,000, resulting in a larger measurable viscous length scale (and less acute spatial resolution issues). Unlike prior PIV experimental campaigns in the HRNBLWT [7, 8, 19] which were tailored to achieve high Re_τ planar PIV databases, the present campaign is tailored to obtain

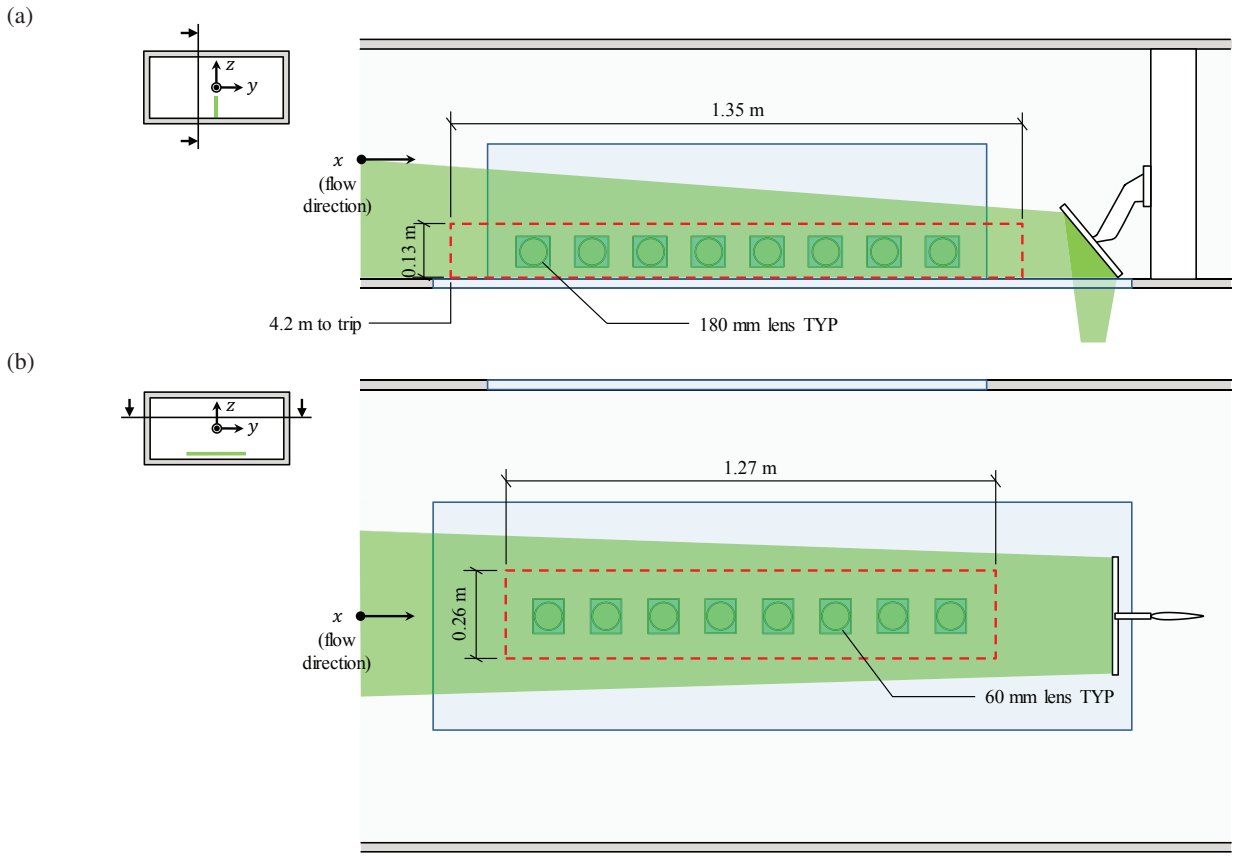

Figure 1: Experimental setup used to conduct large field of view planar PIV experiments in the HRNBLWT. (a) and (b) shows the configuration used to capture a streamwise/wall-normal plane and streamwise/spanwise plane, respectively. The red dashed line corresponds to the field of view captured from the imaging system.

snapshots of very large scale streamwise motions with sufficient fidelity. Hence, experiments are conducted near the upstream end of the test section ($x \approx 4$ m) where the boundary layer thickness is small with a thickness of $\delta \approx 90$ mm (still large relative to many boundary layer facilities, but small compared to what is achieved further downstream in the HRNBLWT). This enables, at moderate Reynolds number, well resolved instantaneous snapshots with a streamwise extent of $O(10\delta)$. To achieve this, the field of view (FOV) is constructed by stitching the imaged region from eight high-resolution 14 bit PCO 4000 PIV cameras. Two camera arrangements are employed (see figure 1); one to quantify velocity fields on a large streamwise/wall-normal—hereafter xz—plane and the other on a streamwise/spanwise — hereafter xy — plane. The red dashed lines in figures 1(a) and (b) show the combined field of view for each arrangement. Table 1 details the key experiment parameters for both arrangements. Each camera has a resolution of 4008×2672 pixels, and is equipped with a 180mm Tamron macro lens for the xz plane measurements, or a Nikon 60mm lens for the xy plane measurement (due to the reduced object distance for this case). Measurements on the xz plane are conducted at three freestream velocities (10, 20 and 30 m/s), with corresponding Reynolds numbers ranges across the extent of the FOV of $Re_\tau \approx 2400 - 2900$, $4800 - 5400$ and $6600 - 7900$, respectively. On the xy plane, only data at $U_\infty \approx 10$ m/s is presented. The present paper will focus primarily on discussion of preliminary results from the xz plane experiment.

Seeding was injected in close proximity to the blower fan but prior to the facility's flow conditioning section. The seeding was circulated throughout the whole laboratory to obtain a homogeneous seeding density across the test section. Particle illumination was provided during measurements by a Big Sky Nd-YAG double pulse laser that delivers 120mJ/pulse. Two plano-convex cylindrical lenses were used to reduce the laser sheet thickness to approximately 1mm, which was then subsequently spread using a plano-concave cylindrical lens with a focal length of −40 mm. To ensure adequate illumination levels across the large streamwise extent of the FOV it was necessary to project the laser sheet upstream through the working section. Consequently, the last optical mirror was placed within the test section of the HRNBLWT (see figure 1). To ensure such an arrangement had no adverse effects on the flow (blockage effects), diagnostic hotwire anemometry measurements were performed; one with the mirror present and one without. These measurements were carried out at matched streamwise position and under equivalent flow conditions as the subsequent PIV measurements. The results revealed good agreement between the two hotwire measurements for the mean flow (maximum percentage difference relative to the freestream velocity of 0.18%) and turbulence intensity levels (maximum percentage difference relative to the maximum turbulence intensity of 0.51%), which indicate that the PIV measurements are a sufficient distance upstream of the optic to avoid any adverse influence. We note that further examination is necessary for the xy plane optical configuration, therefore results from this plane should be considered preliminary at this stage.

Calibration and PIV evaluation

Because multiple cameras are used here to construct a combined FOV, a calibration procedure is essential and needs to account for distortions within the image plane and also provide a means to stitch the velocity fields from each camera. To this end, we utilise a large glass calibration target that spans the entire extent

General parameters	
Vectors per image	$\approx 5\times10^5$
Number of images	3000
Laser sheet thickness	$\approx$ 1mm
Particle size	$\approx 1-2\ \mu$m
Seeding	Polyamide particles
Flow medium	Air
xz-plane parameters	
Field of view	$\approx 1.35\text{m}\times0.13\text{m}$
Depth of field	$\approx$ 1mm
Optical magnification	$\approx 50\mu$m/pixel
xy-plane parameters	
Field of view	$\approx 1.27\text{m}\times0.26\text{m}$
Depth of field	$\approx$ 5mm
Optical magnification	$\approx 67\mu$m/pixel

Table 1: Experimental parameters for the PIV experiments

of the FOV. Printed onto the target is an array of dots, with a spacing between dots of 5 mm (a spacing chosen to provide sufficient dots to quantify the optical distortions induced along the optical path). The target enables us to apply a pixel to real conversion by mapping the pixel space for each camera (X, Z) to real space (x, z) within the tunnel. Additionally, we are able to precisely locate each camera relative to the others, which is essential to stitch the individual vector fields from each camera into the combined FOV.

The image pairs are processed using an in-house PIV package developed at the University of Melbourne [8, 19]. All images are first pre-processed by thresholding the histogram of their CCD intensities, and an average image for each camera is subtracted. Velocity vector evaluation is performed based on a cross-correlation algorithm using multi-grid [23] with window deformation applied at each pass [17]. Two multigrid passes are performed in all measurements, with the final window sizes for each dataset and other processing parameters detailed in table 2. 50% overlap is employed for all images at the final interrogation window size and subpixel vector displacements are computed using a three-point Gaussian fit. It should be noted that since we employ a low magnification level, particle diameters are typically $1-2$ pixels. This size is less than that typically recommended for PIV experiments [2], and therefore can lead to pixel-locking of the velocity fields (a bias error towards integer values) [21]. To minimise this shortcoming, a Gaussian kernel filter is applied to the raw images [2]. Additionally, the window deformation technique used here during vector evaluation is also known to further reduce the influence of pixel-locking [17].

U_∞ (m/s)	Re_τ	ν/U_τ (μm)	Window size l^+	Window size pixels
xz-plane				
10	2400-2900	42	26	32×32
20	4800-5400	22	52	32×32
30	6600-7900	15	75	32×32
xy-plane				
10	2400-2800	42	35	32×32

Table 2: Summary of processing parameters of the experimental data. The friction velocity U_τ is computed at the middle of the FOV.

Results

xz-plane flow statistics

Validation of the xz plane measurements is provided through comparison of single point statistics obtained from the current measurement to both prior hot-wire anemometry datasets and recent direct numerical simulations. For the PIV databases, well converged velocity statistics are obtained from the 3000 statistically independent instantaneous velocity snapshots acquired at each Reynolds number. In the present analysis comparisons are limited to first and second order single point statistics across the entire wall-normal extent of the boundary layer for the xz plane datasets. It should be noted that for consistency δ and U_τ are computed by applying the composite velocity profile of Chauhan *et al.*[6] for all datasets. This yields a boundary layer thickness that is approximately 25% greater than δ_{99}. Additionally, as there is a slow variation of δ across the streamwise extent of the FOV, statistics presented here are computed at the middle of the FOV and are averaged across a streamwise length of approximately δ. Figure 2 presents the mean streamwise velocity profile (U^+), the streamwise and wall-normal turbulence intensities ($\overline{u^2}^+$ and $\overline{w^2}^+$) and the Reynolds shear stress ($-\overline{uw}^+$) for the PIV database at $U_\infty \approx 10$ m/s. Statistical results from recent DNS database at $Re_\tau \approx 2500$ [18] is also included (dashed red lines) for comparison. Because this PIV database and the DNS databases are at matched Re_τ, they provide an appropriate means to benchmark the quality of the experiments, isolating any experimental uncertainties which are not present in DNS.

The flow statistics U^+ and $\overline{u^2}^+$ show good agreement between the DNS dataset and PIV. However, the near wall region $z^+ < 100$ is not clearly captured using the PIV system. For wall-turbulence larger discrepancies are typically present in this region (near-wall region) particularly due to the influence of spatial attenuation and wall reflections. In the case of the PIV measurements the degree of attenuation is a function of the interrogation window size and laser sheet thickness; this shortcoming are not present in the DNS databases. To explore the influence of spatial averaging further, following de Silva *et al.* [8] we spatially box filter the DNS database at matched spatial resolution to the PIV database at $U_\infty \approx 10$ m/s. It is worth highlighting that unlike prior attempts at examining the effect of spatial attenuation on turbulence statistics where different flow geometries or Re_τ are considered [8], here both parameters are matched. The black solid lines in figures 2(b), 2(c) and 2(d) show the turbulence intensity levels obtained from the DNS velocity fields filtered at matched resolution to the PIV database. Good agreement is observed between the PIV and filtered DNS statistics. PIV experiments, however, are subject to two errors (in particular) which have competing effects on measurements of turbulent fluctuations: spatial filtering (via the windowing process) attenuates the magnitude of fluctuations, while measurement noise has the ability to offset this attenuation. In figure 3 the pre-multiplied energy spectra of the streamwise and wall-normal fluctuations are compared between the PIV and DNS databases. Although only two wall-normal locations are shown here for each spectra, the collapse observed between the PIV and DNS data is indicative of that observed across the entire boundary layer. These comparisons indicate that there is very little measurement noise present in the PIV data, which usually manifest as a rapid increase in energy at small wavelengths (see [3]). The good agreement between the PIV and filtered DNS statistics then suggests that the disagreement observed between the PIV and DNS statistics in figure 2 is due almost entirely to spatial averaging of the PIV fields, and that this spatial averaging is well approximated by a box filter.

Figures 4(a) and 4(b) present the same flow statistics as in figure 3 at freestream velocities of $U_\infty \approx 20$ m/s and 30 m/s, respectively. Due to the lack of DNS databases at higher Re_τ comparisons are drawn to single-point hotwire anemometry (HWA) measurements [12]. The results show acceptable agreement between the PIV and HWA datasets for the streamwise fluctuations. It is important to note here that the spatial resolution of

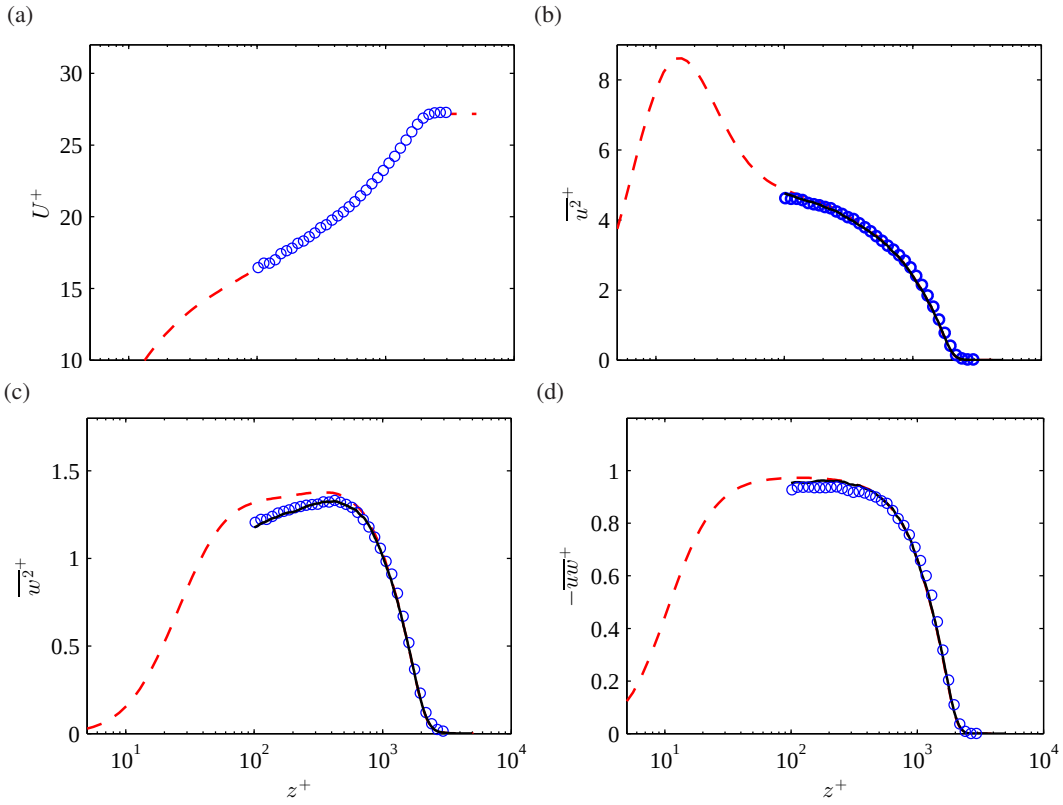

Figure 2: Comparison of flow statistics (a) mean streamwise velocity U^+, (b) streamwise turbulence intensity $\overline{u^2}^+$, (c) wall-normal turbulence intensity $\overline{w^2}^+$ and (d) Reynolds shear stress $-\overline{uw}^+$. The blue ○ symbols correspond to results from PIV database at $U_\infty \approx 10$ m/s, and the dashed lines corresponds to a recent DNS database at $Re_\tau \approx 2500$ [18]. The solid black line in (b-d) corresponds to statistics from the $Re_\tau = 2500$ DNS database filtered to match the spatial resolution of PIV measurement.

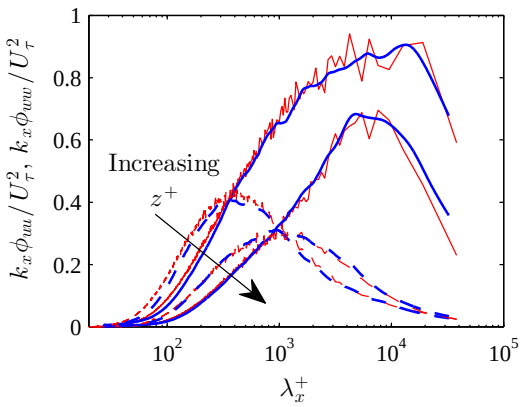

Figure 3: Comparison of the pre-multiplied energy spectra between the PIV ($U_\infty \approx 10$ m/s) and DNS databases which are shown in blue and red, respectively. Solid lines show the spectra of the streamwise velocity fluctuations ($k_x\phi_{uu}/U_\tau$), while dashed lines show the spectra of the wall-normal velocity fluctuations ($k_x\phi_{ww}/U_\tau$). Spectra are shown at $z^+ \approx 200$ and $z^+ \approx 1000$. The arrow shows the direction of increasing z^+.

the PIV data increases by a factor of approximately 1.5 between figures 4(a) and 4(b), while that of the hotwire remains approximately constant at 20 viscous units. This accounts for the larger difference observed between the two measurement techniques in figure 4(b).

Instantaneous velocity fields and spectra

The large spatial extent of the current measurements enable us to visualise large coherent motions known to exist in boundary layers at moderate to high Reynolds number. To demonstrate the value in this, figure 5 provides some sample instantaneous velocity fields, where (a-b) and (c-d) shows a xz and xy planar velocity field, respectively. Colour contours correspond to the streamwise and wall-normal velocity components in (a) and (b), respectively for the xz plane. Similarly (c) and (d) correspond to the streamwise and spanwise velocity components, respectively from the xy plane.

Visual inspection of the velocity fields presented reveals spatial structures over a wide range of length scales, emphasising the importance of large scale measurements with good spatial resolution. For example, the xz plane shows several characteristic features. These include the recurrent patterns of interfacial bulging at the turbulent/non-turbulent interfaces, patches of inclined vortical motions [1], large regions of relatively low turbulence intensities [14] and concentrated regions of high shear [15]. The xy plane shown in figure 5(b) is acquired at the middle of the log region and also reveals important structural features, including elongated streamwise structures exceeding 14δ in length. In fact, there is evidence of coherence in the streamwise velocity that extends beyond the FOV presented here, consistent with previously reported superstructures [11]. It is worth highlighting (although not reproduced in figure 5) that these very large scales regions of coherence are even more discernible by inspecting streamwise velocity fluctuations.

Another notable advantage of the PIV databases is that they can be used to directly compute the energy spectra in the spatial domain over a wide range of scales. Previously, spatial information over streamwise extents larger than a few δ were inferred from temporally resolved point measurements using Taylor's frozen turbulence hypothesis [20]. However, this approach

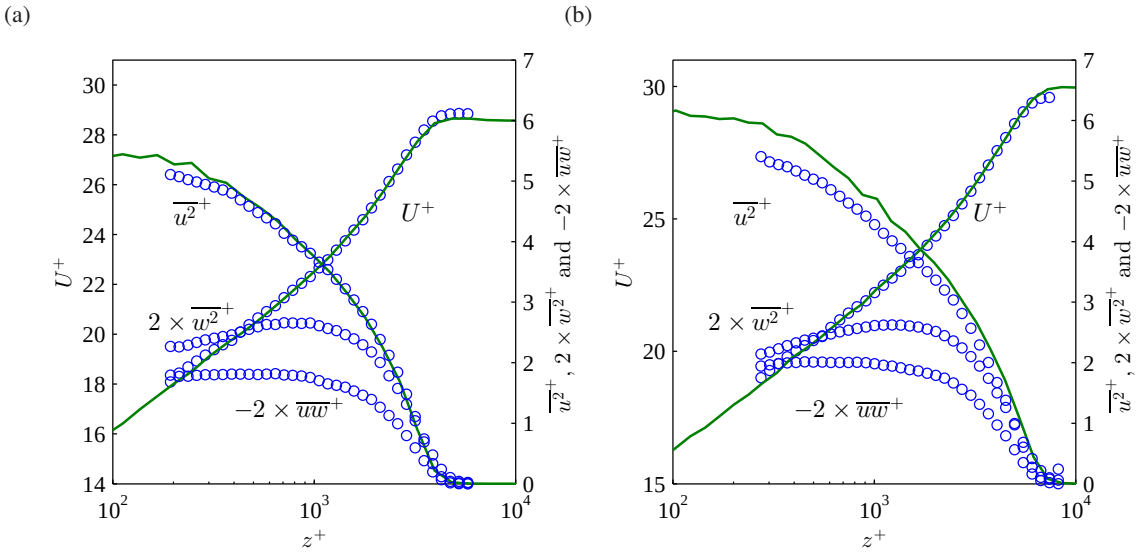

Figure 4: Comparison of flow statistics reproduced from higher Re_τ datasets, where (a) $U_\infty \approx 20$ and (b) $U_\infty \approx 30$. The blue ○ symbols correspond to results from PIV database , and the green solid line represent hot-wire dataset [12] at an equivalent Re_τ to the PIV dataset.

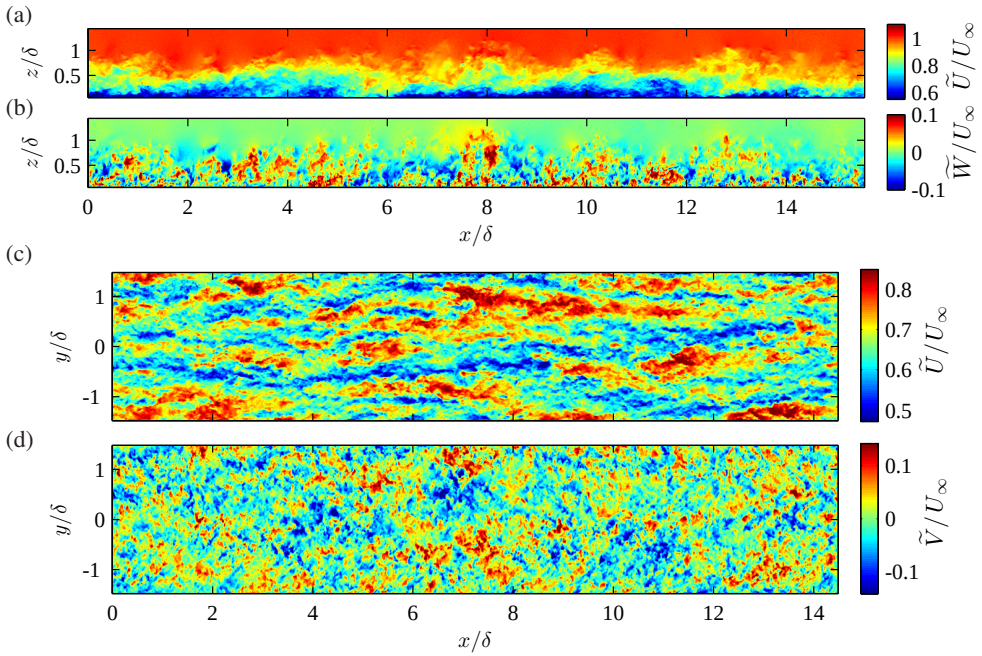

Figure 5: Instantaneous velocity fields from the PIV datasets at $U_\infty \approx 10$ for the (a-b) xz and (c-d) xy plane. Colour contours represent the instantaneous velocity components captured for each configuration, where (a) and (c) shows streamwise velocity, (b) wall-normal velocity and (d) spanwise velocity. Spatial extents are normalised by δ_{99} computed at the middle of each field of view.

is limited, particularly over larger spatial extents [10, 4]. The pre-multiplied energy spectrogram presented in figure 6 shows a direct comparison between a single point hotwire measurement and the PIV database at $U_\infty \approx 20$ m/s. The results show good agreement, closely agreeing with prior work [10], but now over a much larger spatial extent. These results support the use of Taylor's frozen hypothesis in computing the (average) energy spectrum over the streamwise domain size of the PIV measurements presented in this study. The results also indicate that the mean streamwise velocity provides a good estimate of the mean convection velocity for the wall-normal locations captured by the present measurements. One notable shortcoming of the PIV datasets is the missing near-wall information from the PIV databases. Since the range of scales is large in this region and the mean velocity is vanishingly small as the wall is approached, one would expect larger discrepancies when using Taylor's frozen hypothesis to project temporal signals due to larger variations in convection velocities at these scales [4, 9].

Conclusions

This paper presents large scale multi-camera planar PIV measurements, which are tailored to maximise the streamwise FOV while maintaining sufficient spatial resolution to resolve a large proportion of the turbulence intensity in the log region and above. To assess the quality of the experiments, flow statistics from the lowest Re_τ PIV measurement are compared with a recent direct numerical simulation database, revealing good agreement when spatial attenuation of the PIV is accounted for. The spatial attenuation of the PIV is shown to be well approximated by applying a box filter (equal to the interrogation box size of the PIV) to the DNS databases prior to computing flow statistics. Visual examination of instantaneous ve-

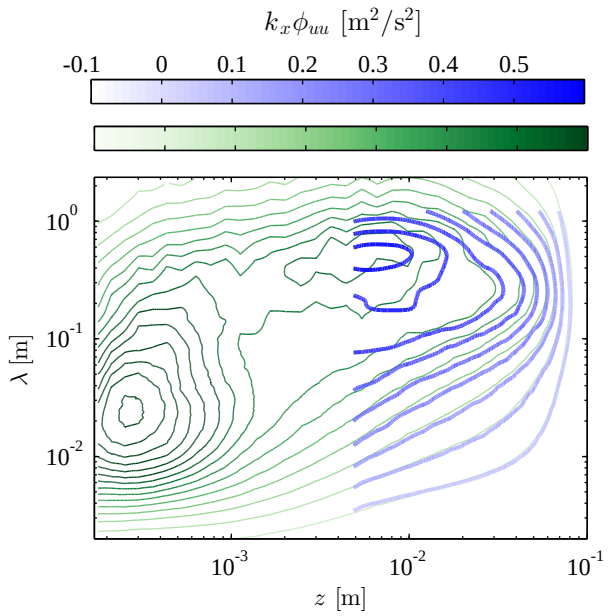

Figure 6: Comparison of pre-multiplied energy spectrogram for the streamwise velocity fluctuations between the PIV database at $U_\infty \approx 20$ m/s (blue contours) and a hotwire anemometry measurement at equivalent Re (green contours).

locity fields from both the streamwise/wall-normal and streamwise/spanwise planes reveal several regular structural features, including coherent motions that extend beyond 10δ in the streamwise direction. Comparisons between the pre-multiplied energy spectra of the streamwise velocity fluctuations from the PIV and hotwire measurements also show good agreement over the field of view when Taylor's frozen turbulence hypothesis is assumed.

This study provides a foundation for similar large scale PIV measurements, enabling future work to be performed into characterising the largest coherent motions prevalent in boundary layers to unravel their dynamics and associated Re_τ trends.

Acknowledgements

The authors wish to gratefully thank the financial support of the Australian Research Council.

References

[1] Adrian, R. J., Meinhart, C. D. and Tomkins, C. D., Vortex organization in the outer region of the turbulent boundary layer, *J. Fluid Mech.*, **422**, 2000, 1–54.

[2] Adrian, R. J. and Westerweel, J., *Particle Image Velcimetry*, Cambridge University Press, 2011.

[3] Atkinson, C., Buchmann, N. A., Amili, O. and Soria, J., On the appropriate filtering of piv measurements of turbulent shear flows, *Exp. Fluids*, **55**, 2014, 1–15.

[4] Atkinson, C., Buchmann, N. A. and Soria, J., An experimental investigation of turbulent convection velocities in a turbulent boundary layer, *Flow, Turb. Comb.*, 1–17.

[5] Bruun, H. H., *Hot-Wire Anemometry: Principles and Signal Analysis*, Oxford University Press, 1995.

[6] Chauhan, K. A., Monkewitz, P. A. and Nagib, H. M., Criteria for assessing experiments in zero pressure gradient boundary layers, *Fluid. dyn. res.*, **41**, 2009, 021404.

[7] de Silva, C. M., Chauhan, K. A., Atkinson, C. H., Buchmann, N. A., Hutchins, N., Soria, J. and Marusic, I., Implementation of large scale PIV measurements for wall bounded turbulence at high Reynolds numbers, 18^{th} Australasian Fluid Mechanics Conference., 2012.

[8] de Silva, C. M., Gnanamanickam, E., Atkinson, C., Buchmann, N. A., Hutchins, N., Soria, J. and Marusic, I., High spatial range velocity measurements in a high reynolds number turbulent boundary layer, *Phys. Fluids*, **26**, 2014, 025117.

[9] del Álamo, J. and Jiménez, J., Estimation of turbulent convection velocities and corrections to Taylor's approximation, *Journal of Fluid Mechanics*, **640**, 2009, 5–26.

[10] Dennis, D. J. C. and Nickels, T., On the limitations of Taylor's hypothesis in constructing long structures in a turbulent boundary layer, *J Fluid Mech*, **614**, 2008, 197–206.

[11] Hutchins, N. and Marusic, I., Evidence of very long meandering features in the logarithmic region of turbulent boundary layers, *J. Fluid Mech*, **579**, 2007, 1–28.

[12] Kulandaivelu, V., *Evolution of zero pressure gradient turbulent boundary layers from different initial conditions*, Ph.D. thesis, The University of Melbourne, 2012.

[13] Marusic, I., Mathis, R. and Hutchins, N., Predictive model for wall-bounded turbulent flow, *Science*, **329**, 2010, 193–196.

[14] Meinhart, C. D. and Adrian, R. J., On the existence of uniform momentum zones in a turbulent boundary layer, *Phy. Fluids*, **7**, 1995, 694.

[15] Priyadarshana, P. J. A., Klewicki, J. C., Treat, S. and Foss, J. F., Statistical structure of turbulent-boundary-layer velocity–vorticity products at high and low reynolds numbers, *J. Fluid Mech.*, **570**, 2007, 307–346.

[16] Raffel, M., Willert, C. E., Wereley, S. T. and Kompenhans, J., *Particle Image Velocimetry - A Practical Guide*, Springer Berlin Heidelberg New York, 2007.

[17] Scarano, F., Iterative image deformation methods in PIV, *Meas Sci Tech.*, **13**, 2001, R1–19.

[18] Sillero, J. A., Jiménez, J. and Moser, R. D., One-point statistics for turbulent wall-bounded flows at reynolds numbers up to $\delta^+ = 2000$, *Phys. Fluids*, **25**, 2013, 105102.

[19] Squire, D. T., de Silva, C. M., Hutchins, N. and Marusic, I., High fidelity spatial measurements at high Reynolds numbers in turbulent boudary layers, 17^{th} Int Symp on Applications of Laser Techniques to Fluid Mechanics, Lisbon, Portugal, 2014.

[20] Taylor, G. I., The spectrum of turbulence, *Proceedings of the Royal Society*, **164**, 1938, 476–490.

[21] Westerweel, J., Fundamentals of digital particle image velocimetry, *Meas Sci Tech.*, **8**, 1997, 1379–1392.

[22] Westerweel, J., Elsinga, G. E. and Adrian, R. J., Particle image velocimetry for complex and turbulent flows, *Ann. Rev. Fluid Mech.*, **45**, 2013, 409–436.

[23] Willert, C., Stereoscopic digital particle image velocimetry for application in wind tunnel flows, *Meas. Sci. Tech.*, **8**, 1997, 1465.